ARTICLES

Surface-Induced Dissociation of the Benzene Molecular Cation in Fourier Transform Ion Cyclotron Resonance Mass Spectrometry

V. Sergey Rakov,* Eduard. V. Denisov, Julia Laskin, and Jean H. Futrell

Pacific Northwest National Laboratory, William R. Wiley Environmental Molecular Sciences Laboratory, P.O. Box 999 (K8-84), Richland, Washington 99352

Received: January 24, 2001; In Final Form: November 29, 2001

Energy transfer in collisions of benzene molecular ions with a fluorinated self-assembled monolayer surface at normal incidence was studied over the range of collision energies from 0 to 75 eV in a Fourier transform ion cyclotron resonance mass spectrometer (FT-ICR MS). Rice−Ramsperger−Kassel−Marcus (RRKM) theory was used to calculate breakdown graphs for a simplified decomposition scheme of benzene on the time scale of ICR MS detection. Statistical partitioning of excess internal energy between the neutral and the ionic products was included in the theoretical model. Internal energy distributions of the predissociating parent ions were iteratively calculated using the recursive internal energy distribution search (RIEDS) method for each collision energy. On the basis of the above measurements, the collision-energy-dependent $E_{SID} \rightarrow E_{int}$ energy conversion efficiency was found to maximize at about 19.5% under the conditions of 31 eV SID collision energy.

Introduction

Tandem mass spectrometry (MS/MS) is routinely used for structural determination of a wide variety of ionic species. Following the primary ion selection, its internal energy can be increased in a controlled manner to induce its dissociation. Recording *m*/*z* of its fragments often enables identification of the primary parent ion's structure. If necessary, the fragments of the precursor ion can be selectively fragmented, in turn, to reveal the structure(s) of the fragments themselves. For stable ionic structures, sufficient internal energy has to be deposited into the ion to induce extensive fragmentation and obtain useful structural information from its dissociation pattern. Ion excitation can be achieved either in the ionization step or later by using a variety of post-ionization excitation techniques such as collisional activation[1,2] and various photoactivation methods.[3−5]

In the past decade, dissociations of molecular ions of large, biologically significant complexes have become the main target of the induced-fragmentation studies in mass spectrometry. In the ion−neutral collision, only a part of the center-of-mass translational energy of the colliding pair, E_{CM}, is converted into internal energy of the active complex, E_{int}, promoting collision-induced dissociation (CID). Additionally, for a given laboratory (LAB) frame energy of collision with a neutral agent the mass of which is lower than that of the ion, the CM collision energy decreases with the ion's mass. For a number of reasons, the amount of CM collision energy transferred into internal energy of the ion in a single collision is often insufficient to reach the decomposition threshold. Multiple collision activation increments internal energy of the ion up to and above the dissociation threshold in consecutive energizing collisions. This process is ion- and conditions-specific and presents a dynamic competition between ion activation and deactivation in each collision event. Multiple-photon activation methods, such as infrared multiphoton dissociation (IRMPD), promote internal energy by a similar stepwise mechanism, without CM limitations and without collisional deactivation. For complex molecules with many oscillators, radiative energy losses compete with slow stepwise activation processes, such as multiple collision CID and IRMPD. Surface-induced dissociation (SID) can, in principle, overcome the limitations of both the single- and the multiple-collision CID (or IRMPD). It realizes one collision act in which the effective mass of the neutral agent can be higher than that of a common neutral gas, thus allowing higher internal energy deposition than single-collision CID (or than absorption of a single photon). On the other hand, the energy promotion process is fast and does not present the dynamic dualism of activation−deactivation, characteristic of multiple-collision CID and IRMPD.

SID was successfully applied to study fragmentation of a wide variety of chemical systems starting from relatively small ions[6−21] and expanding to high-mass biomolecules.[22−25] It has been demonstrated that large internal excitation levels can be easily achieved using ion−surface impact, but the nature of ion activation during the ion−surface interaction is not clearly understood. Self-assembled monolayers (SAMs) of organic two-dimensional crystals[7−11] have proven to be very effective substrates for SID. Fluorinated SAMs are especially effective in this sense because they reduce neutralization of projectile ions in ion−surface collision and provide efficient internal excitation of ions. Initial suggestions that a surface could act as an infinite-mass collider making all of the laboratory-frame (LAB) collision energy available for ion excitation have proven

* To whom correspondence should be addressed. Tel: (509) 376-7207. E-mail: rakov@pnl.gov.

10.1021/jp010245d CCC: $22.00
Published on Web 02/27/2002

to be incorrect. Several studies indicate that the effective mass of fluorinated organic surfaces is fairly low (the reported results vary between 40 and 90 amu).[12−15] We have recently compared SID and multiple-collision CID of small peptides and have demonstrated that internal energy distributions (IEDs) are very similar in SAM-SID and multiple-collision CID with argon.[14,15] On the basis of these results, we suggested that normal-incidence ion−surface collisions with a SAM surface involve multiple interactions of the projectile ion with chemical groups on the surface. These multiple collisions result in a very efficient transfer of impact energy into internal energy of the ion. However, in contrast with the multiple-collision activation, SID is a very fast activation technique, which is advantageous in many analytical applications.

Several instrumental configurations have been employed in SID studies. These include angle-resolved tandem MS instruments that allow variation in positioning of the mass analyzer and the inclination of the surface with respect to the precursor ion beam.[13,26−32] Experiments carried out using these instruments provide valuable information on dynamics of the process and scattering characteristics of SID fragments. However, most SID experiments are carried out in tandem quadrupoles or in time-of-flight/reflectron mass spectrometers with a fixed angle between the incident ion beam, the surface, and the analyzer positioned after the surface. These at best provide a representative sample of the fragment ions, depending on optical settings and the effective detector acceptance angle.

Both of the tandem-MS types mentioned above typically detect fragments formed in microseconds to tens of microseconds after the ion−surface collision. On this detection time scale, complex polyatomic ions require substantial excess internal energy above the dissociation threshold to fragment. This excess internal energy above the dissociation threshold is called the kinetic shift (KS) and historically refers to the microsecond detection time scale. As noted, tandem-in-space SID of complex ions exhibits substantial kinetic shifts, on the order of several tens of electronvolts. On the other hand, in Fourier transform ion cyclotron resonance mass spectrometry (FT-ICR MS or FTMS) experiments, with observation times ranging from milliseconds to many seconds, the kinetic shift is drastically reduced. This enables observation of dissociation of internally excited ions at much lower collision energies than in tandem-in-space instruments. Moreover, high mass resolution and MS/MS capabilities of FT-ICR MS are advantageous for precise identification of fragment ions formed in SID. As opposed to sustained off-resonance irradiation (SORI) CID, which requires long (seconds) pump down delays between ion activation and fragment detection, SID experiments produce fragments under high vacuum, offering immediate mass detection. For these reasons, successful coupling of SID with FT-ICR MS reported by several research groups[33−41] remains an attractive research field.

Earlier, we examined the energy transfer in SID of chromium hexacarbonyl molecular ion[40] using a recursive internal energy distribution search (RIEDS) method. In this method, breakdown curves, which indicate the probability of fragmentation as a function of internal energy at a given delay between the internal excitation and fragment ion detection, are used as the internal energy reference. Because $Cr(CO)_6^+$ does not exhibit a significant kinetic shift, we used experimental photoelectron photoion coincidence (PEPICO) breakdown graphs[43] obtained on a microsecond time scale as the internal energy reference directly for the FT-ICR experiments, which were about a second long. Other research groups also used RIEDS to study fragmentation of metal carbonyls[18,42] and fullerene molecular ions.[29]

In this study, we investigated the energy deposition process observed in fluorinated SAM-SID of the benzene molecular cation. The fragmentation of benzene radical cation has been extensively studied using different experimental and theoretical approaches,[44−52] and the energetics and dynamics of its major fragmentation pathways are well-established. Although a relatively small molecular ion, the benzene molecular ion, $C_6H_6^{+\bullet}$ possesses several features of a "medium-to-large" ionic system. For example, it is tightly bound and exhibits a substantial kinetic shift on a microsecond time scale. Consequently, its fragmentation pattern observed in coincidence experiments on a time scale of several microseconds is expected to differ drastically from that observed in a similar experiment on FT-ICR. For this reason, PEPICO experimental breakdown graphs cannot be used to deduce IEDs in FT-ICR SID. As shown below, the breakdown curves for $C_6H_6^{+\bullet}$ were reliably calculated using Rice−Ramsperger−Kassel−Marcus (RRKM) theory[53] and adjusted to the time-scale of the ICR experiment.

Another feature of a large molecular complex presented by benzene is that several of its neutral fragments can store excess internal energy and reduce that available to drive sequential decomposition of the first generation of SID ionic fragments. We accounted for the internal energy partitioning between dissociation products in two out of six reactions involved in the model. Using these corrections to the established RIEDS method, we construct reliable IEDs for benzene cations in our SID experiments. Both characteristics—accounting for substantial kinetic shift in dissociation patterns and tracking partitioning of internal energy in the fragmentation process—increase significantly with molecular ion complexity. For this reason, examining the influence of these effects in the dissociation of a well-characterized model compound such as benzene provides important insights for understanding SID of larger molecular ions.

Experimental Setup

I. Parent Ion Preparation. A detailed description of the experimental setup for SID experiments using the University of Delaware 7T Bruker BioApex FT-ICR mass spectrometer has been presented elsewhere.[39−41] In brief, FC_{12} alkanethiolate $[CF_3(CF_2)_9C_2H_4SH]$ SAMs were prepared on a solid gold disk soldered onto a copper holder. The surface was positioned 1 mm inside the ICR cell near the rear ICR trapping plate at 90° to the magnetic field and was in electrical contact with the trapping plate. Benzene molecular ions were produced in an external electron impact ionization source using relatively low-energy electrons, that is, 3−4 eV above the ionization threshold. The potential difference across the source elements, the extractor and the repeller, which were separated by ~1 cm, did not exceed 2 V.

II. Parent Ion Transfer. Parent ion kinetic energy was varied by floating the ion source above ground potential using an external power supply. The parent ions were continuously extracted from the source and transferred through the electrostatic ion guide and through the ICR cell onto the SID surface target. The SID collision energy was defined as the difference between the source offset (corrected for a separately measured mode kinetic energy at zero source offset) and the target potential. The modulation of the ion beam was accomplished by applying a differential potential across the paired-lens elements of the ion guide, which resulted in "switching the ion beam off" for the time of ICR excitation and detection. Ions

were typically impacted on the surface for 1 ms, which is much longer than the residence time of both the parent and the fragment ions in the ICR cell. The fragment ions were formed within the ICR cell volume after the parent ions were scattered from the surface. As a result of long ion injections, the ion distribution inside the cell prior to the 7 V dynamic voltage trapping (DVT)[37,39,40] became a steady-state distribution. Consequently, no time-of-flight adjustment to the delay between ion introduction and dynamic voltage trapping was necessary. After dynamic voltage trapping and an additional delay of 10 ms (electronics response time), the ions were excited for detection by broadband chirp excitation. Overall delay between the actual SID and the fragment detection was on the order of 0.1 s.

III. Fragment Ion Axial Velocity and Ion Capture. Capturing ions by rapid increase of the trapping potential to 7 V was found to be quite efficient for normal-incidence SAM-SID studies. It has been shown previously[39−41] that in ICR SID experiments the axial component of the ion's kinetic energy after collision with the surface is below 1 eV and does not depend noticeably on SID collision energy. (The axial velocity component in this case coincides with the velocity component normal to the surface, $v_\perp$). This observation seems to be in contradiction with results from other groups that reported substantially higher kinetic energies of recoiled ions.[18,21] However, these studies report the velocity vector of recoiling ions, rather than $v_\perp$. In contrast with the velocity component parallel to the surface ($v_\parallel$) that depends linearly on the $v_\parallel$ of projectile ions, $v_\perp$ varies very slowly with collision energy. Detailed angular-resolved scattering studies by Herman and coworkers demonstrated that $v_\perp$ is efficiently damped during collision leading to the nonspecular scattering.[32] This study demonstrated that the kinetic energy component normal to the surface is close to 1 eV for fluorinate SAM surfaces. Low kinetic energies of recoiling ions were also demonstrated for the normal-incidence SID in a TOF instrument.[54] In the view of these results and our previous work,[39,40] dynamic voltage trapping (DVT) of the ions in the ICR cell after normal-incidence SAM-SID with dynamic raise of trapping potentials to 7 V is sufficient to capture all fragment ions at all collision energies used in this work.

Collision-Energy-Resolved Fragmentation of Benzene Cation

Figure 1 shows collision-energy-resolved fragmentation efficiency curves of benzene molecular ion obtained from SID mass spectra in the range of collision energies from 0 to 75 eV. As collision energy increases, the parent decomposes to produce $C_6H_5^+$ as the major fragmentation channel. A relatively minor primary reaction product is $C_6H_4^+$, resulting from H_2 loss. Lower-mass fragment ions increase monotonically with further increase of collision energy. At about 25 eV collision energy, $C_4H_4^+$ becomes a dominant fragment and declines at higher energy as it dissociates into $C_4H_3^+$. At even higher energies, $C_4H_3^+$ dissociates into $C_4H_2^+$, which dominates high-energy SID spectra. These observations are in agreement with our previous results[38] and with results obtained by others.[21] Product ions $C_6H_4^+$ ($m/z = 76$) and $C_5H_3^+$ ($m/z = 63$) were observed in both of our previous experiments on the prototype Finnigan FTMS-2000 SID instrument[37,38] and in the present work. However, these ions were not major spectral features and did not exhibit pronounced dependence on collision energy.

Consistent with our earlier FTMS/SID study but in disagreement with other studies of double-quadrupole and TOF SID,[10,19,55]

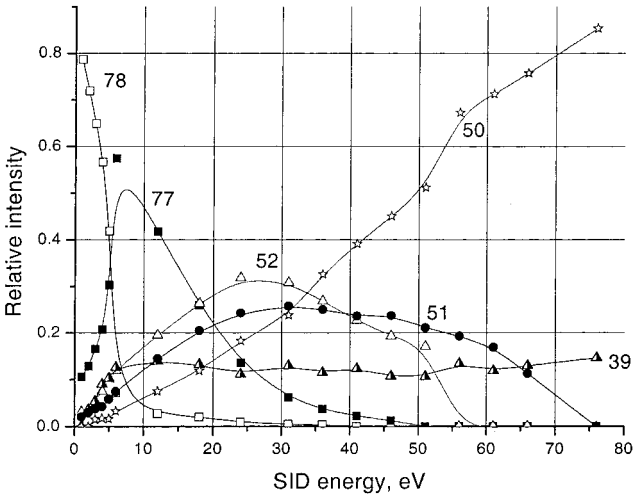

Figure 1. Experimental relative spectral abundances of the normal-incidence SID products of benzene presented as a fragmentogram. The *y* axis represents the SID collision energy defined as a potential difference between the ion source and the SAM-SID surface.

C_2-fragments ($m/z = 26, 27, 28$) were not observed even at high collision energies. The absence of these peaks in our normal-incidence SID experiments[38] was rationalized by suggesting that electronically excited ions generated by high-energy electron impact ionization might be the precursor ions for these dissociative channels. In the present research, ions were intentionally produced using low-energy electron impact ionization. Increasing electron beam energy from below 19 to 70 eV resulted in a significant production of C_2 fragments, both with and without SID collisions. These results support the hypothesis that C_2-fragments ($m/z = 26, 27, 28$) originate from a long-lived electronically excited state(s) of benzene molecular ion, which is significantly populated at high ionizing energy. We also infer from these results that ion−surface impact does not result in electronic excitation of precursor ions in the energy regime studied in this work.

Theoretical Modeling

I. Fragmentation Mechanism and RRKM Model. To model the experimental collision-energy-resolved fragmentation curves of benzene, we have calculated rate constants and breakdown graphs for the following reaction channels:

$$C_6H_6^{+\bullet}\,(78) \rightarrow C_6H_5^{+}\,(77) + H^{\bullet} \quad (1)$$

$$C_6H_6^{+\bullet}\,(78) \rightarrow C_4H_4^{+\bullet}\,(52) + C_2H_2 \quad (2)$$

$$C_6H_6^{+\bullet}\,(78) \rightarrow C_3H_3^{+\bullet}\,(39) + C_3H_3 \quad (3)$$

$$C_6H_5^{+}\,(77) \rightarrow C_4H_3^{+}\,(51) + C_2H_2 \quad (4)$$

$$C_4H_4^{+\bullet}\,(52) \rightarrow C_4H_3^{+}\,(51) + H^{\bullet} \quad (5)$$

$$C_4H_3^{+}\,(51) \rightarrow C_4H_2^{+\bullet}\,(50) + H^{\bullet} \quad (6)$$

Energy-dependent microcanonical rate constants for all reaction channels were calculated using the standard RRKM/QET expression:[53]

$$k(E) = \frac{\sigma W^{\ddagger}(E - E_0)}{h\rho(E)} \quad (1)$$

TABLE 1: RRKM Parameters Used in Calculation of the Rate Constants

reaction	78−77	78−52	78−39	77−51	52−51	51−50
E_0, eV	3.66	4.13	4.19	3.75	2.80	3.95
$\Delta S^{\ddagger}$, J/(mol K)	11.0	43.3	35.4	54.2	33.7	25.0
statistical factor, σ	6	12	12	1	2	1

where $\rho(E)$ is the density of states of the reactant, $W^{\ddagger}(E - E_0)$ is the sum of states of the transition state, E_0 is the critical energy, h is Plank's constant, and σ is the reaction path degeneracy.

Vibrational frequencies, threshold energies, and reaction path degeneracies for reactions 1−4 and 6 were adopted from the literature.[48,56,57] The structure of $C_4H_4^+$, which is a precursor ion for reaction 5, has been extensively discussed in the literature. Two structures of $C_4H_4^+$ formed in unimolecular or collision-induced dissociation of benzene were proposed.[58] Detailed CID studies as well as neutralization−reionization experiments revealed that the two isomers are methylenecyclopropene (I) and vinylacetylene (II).[59−61] Because the linear isomer II is less stable than the cyclic isomer I by 20 kJ/mol, we assumed that a major part of the $C_4H_4^+$ observed in the SID spectra has the methylenecyclopropene structure. Vibrational frequencies of methylenecyclopropene were adopted from ref 62 (Supporting Information). Kinetic energy release measurements indicated that reaction 5 proceeds via a loose transition state.[58] As a result, the critical energy for this reaction can be estimated based on the heats of formation of $C_4H_4^+$ [62] and $C_4H_3^+$.[57] Critical energies and activation entropies for reactions 1−6 are summarized in Table 1. Activation entropies for reactions 5 and 6 were chosen rather arbitrarily. However, because microcanonical rate constants for these reactions rise very sharply with internal energy, the resulting breakdown graphs were not sensitive to the activation entropies for reactions 5 and 6.

II. Internal Energy Partitioning. The internal energy content of fragments formed by reactions 1−3 was calculated on the basis of the following considerations. If the excess internal energy of the precursor ion is statistically partitioned among the fragments, then part of it is deposited as a vibrational excitation of ionic and neutral fragments, while another part is released as the relative kinetic energy of departing fragments. Kinetic energy releases (KER) for reactions 1, 2, and 4 are 63, 26, and 18 meV, respectively.[63] KERs for reactions 2 and 3 are small and can be neglected. However, the internal energy of $C_6H_5^+$ formed by reaction 1 was corrected for the energy released into translation. Partitioning of energy between the ionic and neutral products was included in the modeling as described elsewhere[64] (vibrational frequencies of C_2H_2 were adopted from reference 65). Although the internal energy content of C_4H_3 (m/z = 51) formed via reactions 4 and 5 is different, this difference is small (less than 0.02 eV) at the reaction threshold for the formation of $C_4H_2^+$. Thus reaction 6 was considered as a single channel in the present modeling.

III. Rate Constants, Kinetic Shift, and Breakdown Curves for FTMS and Sector MS. Microcanonical rate constants for internal energies from 0.1 to 30 eV calculated for the reaction scheme outlined above are plotted in Figure 2. The corresponding kinetic equations were numerically integrated using the Runge−Kutta algorithm for each value of internal energy. Breakdown curves obtained for detection times of 10 μs, 100 ms, and 10 s are compared in Figure 3, parts a, b, and c, respectively. They essentially provide better elaboration of the

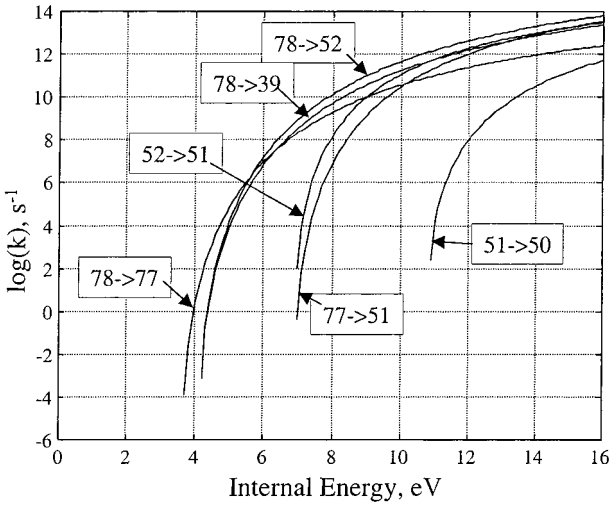

Figure 2. Rate−energy dependencies for reactions 1−6 used in the RRKM modeling.

results depicted in Figure 2. The most drastic differences occur in the abundance of phenyl cation (m/z = 77). At low internal energy (less than 4.5 eV) and long reaction time (Figure 3b,c), the parent ion dissociates exclusively into phenyl cation (m/z = 77). The maximum relative abundance of m/z = 77 is 60% at 10 μs compared to 100% for times longer than 0.1 s. Reaction 2 competes efficiently with reaction 1 only at energies above 4.5 eV. However, the competition between reactions 1 and 2 is much more apparent on a microsecond time scale. The enhanced competition between these two channels results from the crossing of rate−energy curves for these reactions that occurs at a rate constant of 10^6 s^{-1}, corresponding to a reaction time of 1 μs. Further decomposition of phenyl cation into $C_4H_3^+$ has a much lower rate constant at energies below 7 eV and thus is not responsible for the difference in breakdown curves of m/z = 77 in Figure 3 parts a, b, and c. In fact, the rate constant for reaction 4 becomes significant at around 7 eV, causing an abrupt drop in m/z = 77 abundance. Sampling time is a significant factor even for the most energetically demanding decomposition channel of $C_4H_3^{+\bullet} \rightarrow C_4H_2^+ + H^{\bullet}$. As shown, the breakdown curve for $C_4H_2^+$ rises significantly slower at 10-μs detection than at longer times.

The breakdown curve of the parent ion is shifted toward lower energies by about 1 eV for longer sampling times. It is interesting to note that breakdown graphs differ insignificantly for 0.1 and 10 s as indicated by Figure 3, parts b and c. Because our typical SID experiments have detection times on the order of 0.1 s, the breakdown graph shown in Figure 3b was used to estimate benzene internal energy distributions and SID energy transfer efficiency.

IV. Recursive Internal Energy Distribution Search Method. Estimation of internal energy deposition and $E_{SID} \rightarrow E_{int}$ conversion efficiency was done using the recursive internal energy distribution search (REIDS) described in detail elsewhere.[40−42] This is a preferred alternative to the "thermometer ion" method[66] and deconvolution method.[67] Provided the fundamental assumption of statistical theories of kinetics (RRKM, QET), that fragmentation is a function of internal energy and independent of mode of energy deposition, a high degree of precision is enabled by this method. In RIEDS, the energy distribution function of a precursor ion is given by a probability function $P(E)$ of a known analytical form characterized by a set of parameters. Provided the internal-energy dependent fragmentation probability of the precursor ion, $F(E,t)$,

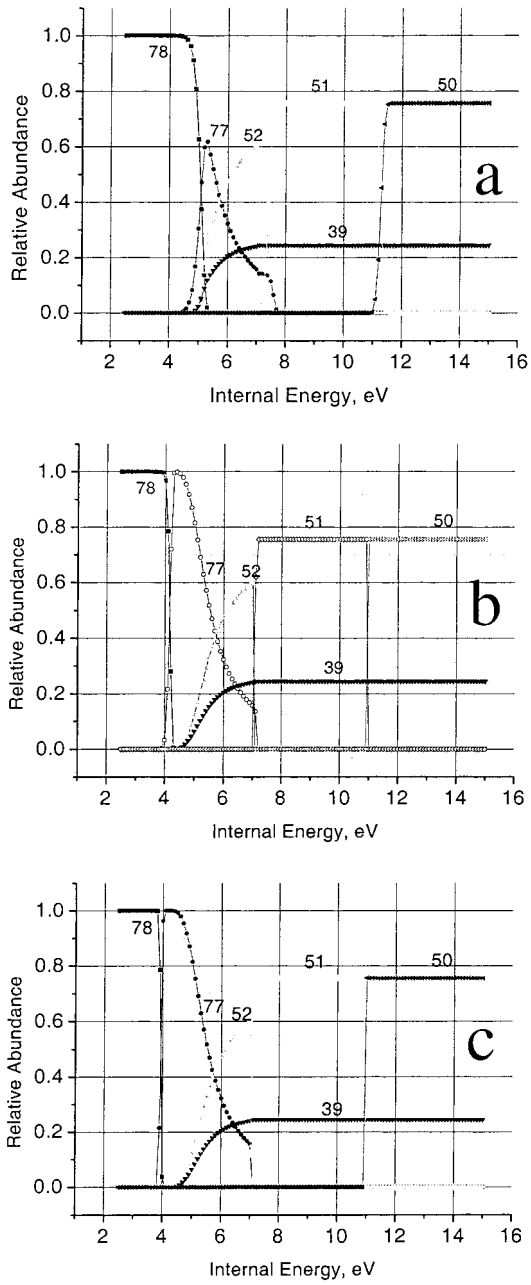

Figure 3. Calculated breakdown graphs for dissociation of benzene radical cation at three different reaction times: (a) at 10 μs; (b) at 0.1 s; (c) at 10 s. The RRKM calculation used threshold energies and entropies summarized in Table 1.

is known, the intensity of the *n*th fragment in the mass spectrum can be calculated from

$$I_n^{\mathrm{pr}} \propto \int_0^{\infty} P(E) F_n(E,t)\, \mathrm{d}E \qquad (2)$$

It follows that for each trial *P(E)* internal energy distribution function, we can create a set of predicted fragment intensities, I_n^{pr}. Minimizing the squared residual sum function gives

$$Q = \sum_{n=0}^{N} (I_n^{\mathrm{exp}} - I_n^{\mathrm{pr}})^2 \qquad (3)$$

where $\{I_n^{\mathrm{exp}}\}$ is the experimental spectrum set of intensities, against the parameters of the $P(E)$ function; we search for the energy distribution function, $P(E)$, that minimizes the difference between $\{I_n^{\mathrm{exp}}\}$ and $\{I_n^{\mathrm{pr}}\}$. In this approach, $P(E)$ is treated as a discrete functional, and the only limitations on the resulting $P(E)$ are those fixed by choosing the analytical form for the internal energy distribution (IED).

The choice of the analytical form for the IED is important in RIEDS analysis. It has to reflect the physics of the excitation process, taking into account mechanisms of activation and deactivation, internal mode coupling, etc. Several candidates for the IED have been suggested previously for activated dissociation studies. Beck et. al.[29] used the Gaussian IED for the SID of C_{60}^+ on highly oriented pyrolitic graphite. Fragmentation modeling provided good correlation between experimental and calculated spectra. Zhang[42] used a linear combination of two Gaussians to interpret energy distributions in exothermic charge exchange reactions of $Fe(CO)_5^+$ with atomic and diatomic molecular ions. This treatment correctly described dissociation originating from two discrete electronic hypersurfaces. Because our parent ion beam was produced under conditions specifically chosen to minimize electronic excitation, we did not anticipate excited electronic states.

The functional form chosen in the present study is similar to the IED used by us previously in our study on the fragmentation of protonated dialanine.[14] This form is an asymmetric Gaussian distribution with three parameters:

$$P(E_{\mathrm{int}}) = \frac{1}{\sqrt{2\pi\sigma}}\, \mathrm{e}^{-(E_{\mathrm{int}}{}^{k} - E_0)^2/(2\sigma^2)} \qquad (4)$$

where k, E_0, and σ are the parameters against which the least-squares fit procedure using Q from eq 3 is performed. Parameter k allows the distribution to be skewed to the right or to the left. Analytical form 4 was successfully used to model IED corresponding to collision-energy-resolved mass spectra of benzene in a range of collision energies between 10 and 55 eV. Alternative forms of the IED were also investigated and did not provide a better fit to our experimental data. Formally, RIEDS is limited by the number of fitting points, for example, fragments in the spectrum. The number of parameters to be used in the analytical form of the internal energy distribution must not exceed the number of peaks in the mass spectrum. For example, to fit a spectrum with six features (parent and five fragments), a function with up to five parameters can be used. Zero-intensity peaks can still be used in the fit, but a spectrum with very few peaks presents a degraded set of variables to a fitting eigenvalue problem, making the latter underdetermined. At collision energies above 55 eV, only three product ions are observed in the experimental SID spectra and the RIEDS definition of IED using an analytical form with three parameters becomes ambiguous. In general, it is desirable to minimize the number of parameters in the analytical form of the internal energy distribution.

Results: Internal Energy Deposition, $E_{\mathrm{SID}} \rightarrow E_{\mathrm{int}}$ Conversion

We performed RIEDS modeling using breakdown graphs shown in Figure 3b. These graphs were calculated using values for threshold energies and entropies listed in Table 1. Figure 4 summarizes the results of the REIDS for benzene spectra at several SID collision energies. Convergence was reached at the tolerance level of 1% (as a ratio of the residual-module sum over the sum of fragment intensities) in all cases. The most probable internal energy shifts to higher values as the SID energy increases, while the $P(E_{\mathrm{int}})$ distribution significantly broadens. The most probable internal energy as a function of

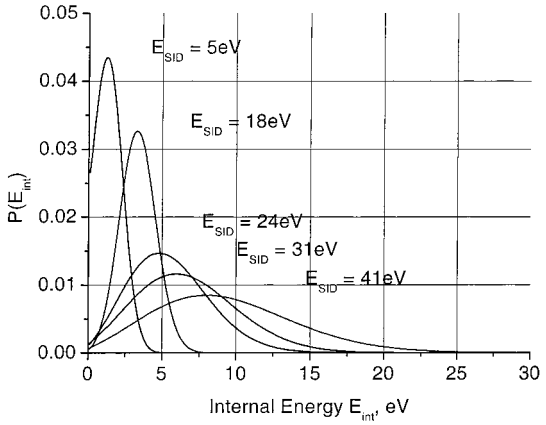

Figure 4. Normalized internal energy distributions obtained using RIEDS for several SID collision energies (shown on the graph). A kinetic delay of 0.1 s was used in solving formal kinetics equations.

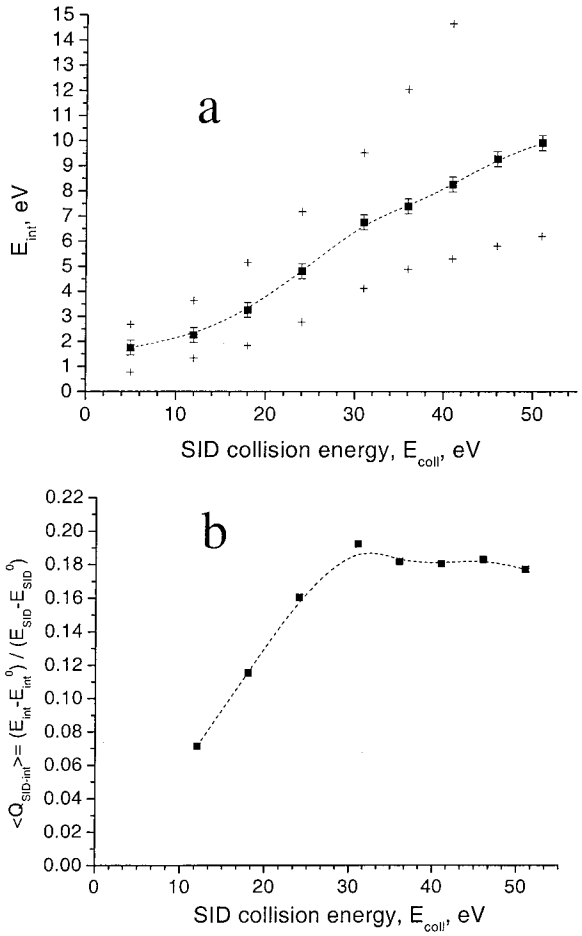

Figure 5. The most probable internal energy (a) deposited by ion-surface impact as a function of SID collision energy (■). The error bars were determined from the sensitivity analysis (see text for details); crosses indicate distribution widths at half-maximum. Panel b shows the efficiency of the kinetic-to-internal energy transfer as a function of SID collision energy.

SID collision energy is plotted in Figure 5a. Solid squares correspond to the most probable internal energies extracted from IEDs calculated using RRKM parameters from Table 1. Crosses indicate IED widths at half-maximum. As mentioned above, at collision energies above 55 eV, internal energy assignment by RIEDS (for a three-parameter analytical form of IED) becomes inaccurate and, therefore, these data were not plotted in Figure 5a.

We have performed a sensitivity analysis to estimate the uncertainty introduced into RIEDS simulations by the uncertainty in RRKM parameters. RRKM parameters of the first three reactions, 1, 2, and 3, have the most pronounced effect on the predicted mass spectrum. While together these reactions contribute to the overall decomposition of the parent ion, their competition determines relative abundances of $C_6H_5^{+\bullet}$, $C_4H_4^+$, and $C_3H_3^+$ in the mass spectrum. The sensitivity analysis was performed by varying threshold energies of reactions 1−3 by 0.1 eV and activation entropies by 5 J/(mol K). Slowing down one reaction relative to the other had such a dramatic effect on the relative abundance of $C_6H_5^{+\bullet}$, $C_4H_4^+$, and $C_3H_3^+$ in calculated mass spectra that experimental results could not be fitted by theoretically predicted spectra using any IEDs. A good fit could be obtained only by changing RRKM parameters of all primary reactions in one direction. Changes in the most probable internal energies caused by our sensitivity test were on the order of 0.2 eV. Because all of the competing channels were accelerated or decelerated simultaneously by this approach, widths of IEDs were not affected. The error bars shown in Figure 5a reflect the IED modes as a response to variation of the RRKM parameters. It should be noted that the uncertainty in the most probable energy does not exceed a few percent of the distribution width, even at low collision energies.

The average percent of $E_{SID} \rightarrow E_{int}$ transfer extracted from the data in Figure 5a is 19% ± 2%. This value can be obtained as a slope of linear fit for the internal vs collision energy. It is in good agreement with $E_{SID} \rightarrow E_{int}$ transfer efficiencies reported in the literature, which vary from 18−28% for fluorinated SAMs to 12−17% for alkanethiolate surfaces.[67] Our value is also in good agreement with the values determined for other systems on the same instrument (19%, on average, for $Cr(CO)_6^+$;[40,41] 21% for protonated dialanine[14]).

However, there is no physical reason to expect constant energy transfer efficiency in SID experiments for all projectile ions and SID targets. Even for a given ion−surface pair, strict linearity of the internal energy vs collision energy would imply not only the same mechanism of the energy transfer across the whole range of collision energies but also conservation of the rate of the energy transfer. However, factors determining the energy transfer rate may themselves depend on the collision energy. In the past, we pointed out that curves of E_{int} versus E_{SID} observed by most SID researchers, even where reported as linear, in fact have nonlinear trends.[13,33,67,etc] Molecular dynamics simulations also suggest decrease in the energy transfer efficiency with increase in collision energy.[68,69]

By extrapolating the nonlinear curve shown in Figure 5a to $E_{SID} = 0$, we can obtain a positive intercept at $E_{int}^0 \approx 1.75$ eV, which can logically be interpreted as the average initial excitation of benzene ions obtained by low-energy electron impact ionization in our experiments. This initial excitation was present in the projectile ions at all collision energies and should be subtracted from E_{int} in analysis of the $E_{SID} \rightarrow E_{int}$ transfer efficiency. On the other hand, collision energy in our experiments was defined as a potential difference between the source and the SID target. Real electrostatic potentials and special distribution of charges inside the ion source can be quite complicated and introduce an uncertainty in the potential energy of the parent ions of the order of potentials applied to the source lens. Fortunately, because all of the ion source elements were floated above ground potential by the same voltage supply, the uncertainty in E_{SID} is conserved for all collision energies. Thus, the first value of $E_{SID} = 5$ eV can be subtracted from E_{SID} to correct for the ion-source space-charge uncertainty effect.

Subtracting the first data point (E_{int}, E_{SID}) = (5, 1.75 eV) from the data shown in Figure 5a formally "redefines" the coordinate origin of the $E_{int}(E_{SID})$ graph. This approach eliminates errors in the assignment of projectile ion kinetic energy as well as its initial internal excitation and defines $E_{SID} \rightarrow E_{int}$ transfer efficiency as $\langle Q_{SID-int} \rangle = (E_{int} - E^0_{int})/(E_{SID} - E^0_{SID})$, that is, the current ratio of internal-to-collisional energies with the coordinate-origin correction.[40] The $E_{SID} \rightarrow E_{int}$ transfer efficiency calculated in this way and shown in Figure 5b reached its maximum value of ~19.5% at around 31 eV collision energy. We note that significant uncertainty is introduced in the $E_{SID} \rightarrow E_{int}$ efficiency as defined above in calculating slope of the curve shown in Figure 5a. A small variation in the slope assignment of the $E_{int}(E_{SID})$ graph can drastically change the energy transfer efficiency.

Summary

This study is a part of our continuing investigation of SID reaction dynamics. Previously, we addressed in detail the instrumental principles behind successful realization of the SID experiment in FT-ICR and reported the results of SID-energetics studies of the rapidly dissociating $Cr(CO)_6^+$ "thermometer" ion. In the present study, we considered the importance of kinetic shift and kinetic delay between excitation of the parent ion and detection of its fragments, using a well-studied case of benzene molecular cation. RRKM-predicted breakdown curves within a chosen decomposition scheme show a kinetic shift of about 1 eV, which necessitates the use of proper time-scaled dissociation curves in internal energy deposition assignment by the RIEDS method. Those curves show pronounced differences predicted for the breakdown curves (and thus the expected fragmentation spectra) within 10 μs and 0.1 s after the instant energy internal deposition occurs. Further increase of delay time between SID excitation and fragment detection does not result in a significant shift of the breakdown curves. This time scale becomes especially important in the study of energetics of singly protonated peptides SID that is currently in preparation for publication.

Another aspect not accounted for in our previous $Cr(CO)_6^+$ study, but modeled in this work, is internal energy partitioning between ionic and neutral products in chosen reactions. In the present research, it was modeled and taken into account in the process of assignment of the internal energy deposition and breakdown curve prediction. This correction becomes important when neutral products are able to store significant amounts of vibrational excitation, which is certainly true for even larger systems. $E_{SID} \rightarrow E_{int}$ conversion efficiency was found to be collision-energy-dependent with a maximum of about 19.5% at collision energy on the order of 30 eV. Both kinetic shift and energy partitioning are critically important in the SID of complex ions. Future research will consider these effects for the dissociation of model peptides.

Acknowledgment. The authors gratefully acknowledge scientific collaboration with Professor V. Wysocki, whose research team provided us with their samples for the SAMs preparation and expertise in general aspects of SID. We also acknowledge support from DOE, Grant DE-FG02-97ER14813, and NSF, Grant CHE-9616711.

References and Notes

(1) Shukla, A. K.; Futrell, J. H. *Mass Spectrom. Rev.* **1993**, *12*, 211.
(2) Gauthier, J. W.; Trautman, T. R.; Jacobson, D. B. *Anal. Chim. Acta* **1991**, *246*, 211.
(3) McLafferty, F. W. *Acc. Chem. Res.* **1994**, *27*, 379.
(4) Dienes, T.; Pastor, S. J.; Schuzch, S.; Scott, J. R.; Yao, J.; Cui, S. L.; Wilkins, C. L. . *Mass Spectrom. Rev.* **1996**, *15*, 163.
(5) Williams, E. R. *Anal. Chem. News and Features* **1998**, 179A.
(6) Cooks, R. G.; Ast, T.; Mabud, Md. A. *Int. J. Mass Spectrom. Ion Processes* **1990**, *100*, 209.
(7) Winger, B. E.; Julian, R. K., Jr.; Cooks, R. G.; Chidsey, C. E. D. *J. Am. Chem. Soc.* **1991**, *113*, 8967.
(8) Wysocki, V. H.; Jones, J. L.; Ding, J. M. *J. Am. Chem. Soc.* **1991**, *113*, 8969.
(9) Morris, M.; Riederer, D. E., Jr.; Winger, B. E.; Cooks, R. G.; Ast, T.; Chidsey, C. E. D. *Int. J. Mass Spectrom. Ion Processes* **1992**, *122*, 181.
(10) Somogyi, A.; Kane, T. E.; Ding, J. M.; Wysocki, V. H. *J. Am. Chem. Soc.* **1993**, *115*, 5275.
(11) Kane, T. E.; Samogyi, A.; Wysocki, V. H. *Org. Mass Spectrom.* **1993**, *28*, 283.
(12) Minton, T. K.; Giapis, K. P.; Moore, T. *J. Phys. Chem. A* **1997**, *101*, 6549.
(13) Koppers, W. R.; Beijersbergen, J. H. M.; Weeding, T. L.; Kistemaker, P. G.; Kleyn, A. W. *J. Chem. Phys.* **1997**, *107* (24), 10736.
(14) Laskin, J.; Denisov, E.; Futrell, J. H. *J. Am. Chem. Soc.* **2000**, *122*, 9703.
(15) Laskin, J.; Denisov, E.; Futrell, J. H. *J. Phys. Chem. B* **2001**, *105*, 1895.
(16) Christen, W.; Even, U.; Raz, T.; Levine, R. D. *J. Chem. Phys.* **1998**, *108* (24), 10262.
(17) Schultz, D. G.; Hanley, L. *J. Chem. Phys.* **1998**, *109* (24), 10976.
(18) Burroughs, J. A.; Wainhaus, S. B.; Hanley, L. *J. Phys. Chem.* **1994**, *98*, 42, 10913.
(19) Maaijer-Gielbert, J.; Bejersbergen, J. H. M.; Kistemaker, P. G.; Weeding, T. L. *Int. J. Mass Spectrom. Ion Processes* **1996**, *153*, 119.
(20) Braitbart, O.; Tobita, S.; Roy, P.; Nenner, I.; Lablanquie, P.; Hagan, D.; Leach, S. *Int. J. Mass Spectrom. Ion Processes* **1993**, *124*, 185.
(21) Schultz, D. G.; Lim, H.; Gabris, S.; Hanley, L. *J. Mass Spectrom.* **1999**, *34*, 217.
(22) Klassen, J. S.; Kebarle, P. *J. Am. Chem. Soc.* **1997**, *119*, 6552.
(23) Dongre, A. R.; Somogyi, A.; Wysocki, V. H. *J. Mass Spectrom.* **1996**, *31*, 339.
(24) McCormack, A. L.; Somogyi, A.; Dongre, A. R.; Wysocki, V. H. *Anal. Chem.* **1993**, *65*, 2859.
(25) Dongre, A. R.; Jones, J. L.; Somogyi, A.; Wysocki, V. H. *J. Am. Chem. Soc.* **1996**, *118*, 8365.
(26) Worgotter, R.; Kubista, J.; Zabka, J.; Dolejsek, Z.; Mark, T. D.; Herman, Z. *Int. J. Mass Spectrom. Ion Processes* **1998**, *174*, 53.
(27) Sen, A. D.; de Clercq, H. L.; Rakov, V. S.; Shukla, A. K.; Futrell, J. H. *Proc. 46th ASMS Conf. Mass Spectrom. Allied Top.* **1998**, 73.
(28) Mair, C.; Fiegele, T.; Biasioli, F.; Futrell, J. H.; Herman, Z.; Mark, T. D. *Int. J. Mass Spectrom.* **1999**, *185*−*187*, 195.
(29) Beck, R. D.; Rockenberger, J.; Weis, P.; Kappes, M. M. *J. Chem. Phys* **1996**, *104* (10), 3638.
(30) Koppers, W. R.; Tsumori, K.; Beijersbergen, J. H. M.; Weeding, T. L.; Kistemaker, P. G.; Kleyn, A. W. *Int. J. Mass Spectrom. Ion Processes* **1998**, *174*, 11.
(31) Koppers, W. R.; Gleeson, M. A.; Lourenco, J.; Weeding, T. L.; Los, J.; Kleyn, A. W. *J. Chem. Phys.* **1999**, *110* (5), 2588.
(32) Kubista, J.; Dolesek, Z.; Herman, Z. *Eur. Mass Spectrom.* **1998**, *4*, 311.
(33) Ijames, C. F.; Wilkins, C. L. *Anal. Chem.* **1990**, *62*, 1295.
(34) Castoro, J. A.; Nywaysir, L. M.; Ijames, C. F.; Wilkins, C. L. *Anal. Chem.* **1992**, *64*, 2238.
(35) Castoro, J. A.; Rucker, P. V.; Wilkins, C. L. *J. Am. Soc. Mass Spectrom.* **1992**, *3*, 445.
(36) Chorush, R. A.; Little, D. P.; Beu, S. C.; Wood, T. D.; McLafferty, F. W. *Anal. Chem.* **1995**, *67*, 1042.
(37) Rakov, V. S.; Futrell, J. H.; Nikolaev, E. N.; Wronka, J. *Proc. 46th ASMS Conf. Mass Specrom. Allied Top.* **1998**, 901.
(38) Zhong, W.; Nikolaev, E. N.; Futrell, J. H.; Wysocki, V. H. *Anal. Chem.* **1997**, *69*, 2496.
(39) Rakov, V. S.; Futrell, J. H.; Denisov, E. V.; Nikolaev E. N. *Eur. Mass Spectrom.* **2000**, *6*, 299.
(40) Rakov, V. S.; Denisov, E. V.; Futzell, J. H.; Ridge, D. P. *Int. J. Mass Spectrom. Ion Processes* **2002**, *213*, 25.
(41) Rakov, V. S. Ph.D. Thesis, University of Delaware, Newark, Delaware, Fall 1999.
(42) Zhang, T. Ph.D. Thesis, University of Delaware, Newark, Delaware, Fall 1995.
(43) Elan, J. H. D.; Frey, R.; Shulte, H.; Brehm, B. *Int. J. Mass Spectrom. Ion Processes* **1976**, *21*, 209.
(44) Rosenstock, H. M.; McCulloh, K. E.; Lossing, F. P. *Int. J. Mass Spectrom. Ion Phys.* **1997**, *25*, 327.
(45) Baer, T.; Willett, G. D.; Smith, D.; Phillips, J. S. *J. Chem. Phys.* **1979**, *70*, 4076.
(46) Andlauer, B.; Ottinger, Ch. *Z. Naturforsch.* **1972**, *27A*, 293.

(47) Lifshitz, C.; Mackenzie Peers, A.; Weiss, M.; Weiss, M. J. *Adv. Mass Spectrom.* **1974**, *6*, 87.
(48) Kühlewind, H.; Kiermeier, A.; Neusser, H. J. *J. Chem. Phys.* **1986,** *85*, 4427.
(49) Grebner, Th. L.; Neusser, H. J. *Int. J. Mass Spectrom. Ion Processes* **1999**, *185/186/187*, 517.
(50) Klippenstein, S. J.; Faulk, J. D.; Dunbar, R. C. *J. Chem. Phys*. **1993**, *98*, 243.
(51) Van der Hart, W. J. *Int. J. Mass Spectrom. Ion Processes* **1994**, *130*, 173.
(52) Van der Hart, W. J. *Int. J. Mass Spectrom.* **1998**, *176*, 23.
(53) Robinson, P. J.; Holbrook, K. A. *Unimolecular Reactions*; Wiley-Interscience: London, 1972.
(54) Leigh, N. D.; Riederer, D. E. *Proc. 49th ASMS Conf. Mass Spectrom. Allied Top.* **2001**.
(55) Wysocki, V.; Futrell, J. H.; Rakov, V. S. Private communication.
(56) Lifshitz, C.; Gibson, D.; Levsen, K.; Dotan, I. *Int. J. Mass Spectrom Ion Phys.* **1981**, 40.
(57) Laskin, J.; Byrd, M.; Futrell, J. H. *Int. J. Mass Spectrom. Ion Processes* **2000**, *195/196*, 285.
(58) Lifshitz, C.; Gibson, D.; Levsen, K. *Int. J. Mass Spectrom Ion Phys.* **1980**, *35*, 365.
(59) Wagner-Redeker, W.; Illies, A. J.; Kemper, P. R.; Bowers, M. T. *J. Am. Chem. Soc*. **1983**, *105*, 5719.
(60) Zhang, M.-Y.; Wesdemiotis, C.; Marchetti, M.; Danis, P. O.; Ray, J. C., Jr.; Carpenter, B. K.; McLafferty, F. W. *J. Am. Chem. Soc.* **1989**, *111*, 8341.
(61) Zhang, M.-Y.; Carpenter, B. K.; McLafferty, F. W. *J. Am. Chem. Soc.* **1991**, *113*, 9499.
(62) Data from NIST Standard Reference Database 69, February 2000 Release, NIST Chemistry WebBook.
(63) Jones, E. G.; Bauman, L. E.; Beynon, J. H.; Cooks, R. G. *Org. Mass Spectrom*. **1973**, *7*, 185.
(64) Laskin, J.; Futrell, J. H. *J. Phys. Chem. A* **2000**, *104*, 5484.
(65) Shimanouchi, T. *J. Phys. Chem. Ref. Data* **1972**, *6*, 993.
(66) Wysocki, V. H.; Kenttamaa, H. I.; Cooks, R. G. *Int. J. Mass Spectrom. Ion Processes* **1987**, *75*, 181.
(67) Vekey, K.; Somogyi, A.; Wysocki, V. H. *J. Mass Spectrom.* **1995**, *30*, 212.
(68) Bosio, S. B. M.; Hase, W. L. *Int. J. Mass Spectrom. Ion Processes* **1998**, *174*, 1.
(69) Schultz, D. G.; Wainhaus, S. B.; Hanley, L.; de Sainte Claire, P.; Hase, W. L. *J. Chem Phys*. **1997**, *106* (24), 10337.